JACS
JOURNAL OF THE AMERICAN CHEMICAL SOCIETY

pubs.acs.org/JACS
Article

Chemistry of the Au−Thiol Interface through the Lens of Single-Molecule Flicker Noise Measurements

Umar Rashid, William Bro-Jørgensen, KB Harilal, PA Sreelakshmi, Reetu Rani Mondal, Varun Chittari Pisharam, Keshaba N. Parida,* K. Geetharani,* Joseph M. Hamill,* and Veerabhadrarao Kaliginedi*

Cite This: https://doi.org/10.1021/jacs.3c14079

ABSTRACT: Chemistry of the Au−S interface at the nanoscale is one of the most complex systems to study, as the nature and strength of the Au−S bond change under different experimental conditions. In this study, using mechanically controlled break junction technique, we probed the conductance and analyzed Flicker noise for several aliphatic and aromatic thiol derivatives and thioethers. We demonstrate that Flicker noise can be used to unambiguously differentiate between stronger chemisorption (Au−SR) and weaker physisorption (Au−SRR′) type interactions. The Flicker noise measurements indicate that the gold rearrangement in chemisorbed Au−SR junctions resembles that of the Au rearrangement in pure Au−Au metal contact breaking, which is independent of the molecular backbone structure and the resulting conductance. In contrast, thioethers showed the formation of a weaker physisorbed Au−SRR′ type bond, and the Flicker noise measurement indicates the changes in the Au-anchoring group interface but not the Au−Au rearrangement like that in the Au−SR case. Additionally, by employing single-molecular conductance and Flicker noise analysis, we have probed the interfacial electric field-catalyzed ring-opening reaction of cyclic thioether under mild environmental conditions, which otherwise requires harsh chemical conditions for cleavage of the C−S bond. All of our conductance measurements are complemented by NEGF transport calculations. This study illustrates that the single-molecule conductance, together with the Flicker noise measurements can be used to tune and monitor chemical reactions at the single-molecule level.

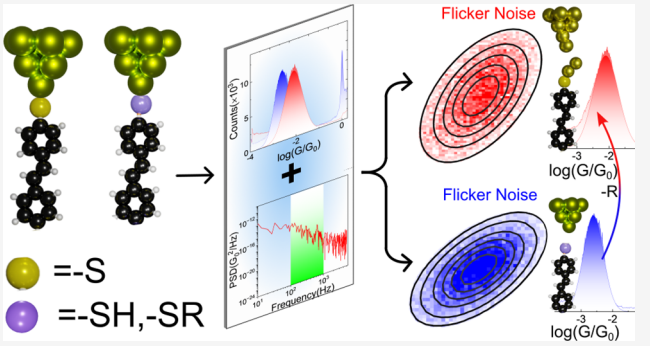

INTRODUCTION

The Au−thiol (Au−S) bond has long been discussed in experimental and theoretical studies owing to its importance in biosensing,[1,2] nanomedicine,[3] drug delivery,[4] molecular electronics,[5−11] molecular spintronics,[12−14] molecular recognition,[15,16] and noble metal nanoparticle catalysis.[7,17] Au−S interactions are used to stabilize different sizes of Au nanoclusters by passivating with thiolate ligands, giving a platform to study different aggregates of metal atoms with a myriad of functionalities.[7] Self-assembled monolayers of thiol-anchored molecules on an Au surface have been the most characteristic systems studied for molecular scale devices for decades.[5,18] A number of surface analysis techniques like X-ray photoelectron spectroscopy (XPS),[19−21] near-edge X-ray absorption fine structure measurements (NEXAFS),[22] scanning tunneling microscopy (STM),[23,24] auger electron spectroscopy (AES),[25] temperature-programmed desorption (TPD),[25,26] high-resolution electron energy loss spectroscopy (EELS),[25] and X-ray diffraction (XRD)[27] have been used to study the intricate nature of Au−S bonding under different environmental conditions.[7,28] Comparing various experimental observations with theoretical predictions to arrive at a common consensus on the structure of the Au−S interface poses a challenge in itself, even though comparisons have been rigorously attempted. However, understanding the nature and geometry of the Au−S interface is critical in designing new synthesis techniques and developing new systems with potential applications. The nature of the bonding is also the deciding factor for the reactivity of these interfaces, and conversely, the mechanism and the nature of products formed when Au−S interfaces are subjected to chemical reactions.[28]

Au−S bond formation involves different kinds of interatomic chemical (covalent and ionic bonding) and physical (van der Waals dispersion forces) interactions, and the interplay of these interactions decides the structural, physicochemical, and

Received: December 13, 2023
Revised: February 1, 2024
Accepted: February 1, 2024

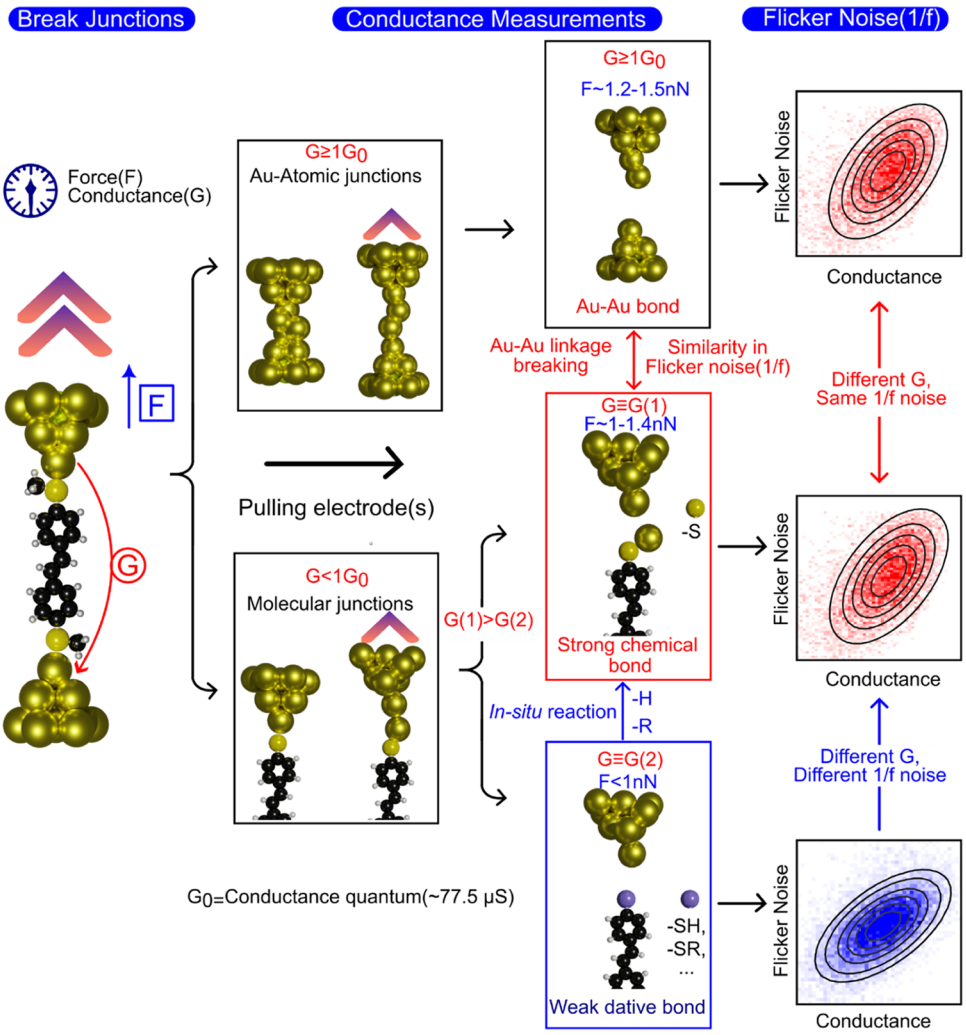

Figure 1. Schematic representation of different single-molecule break junction experimental scenarios. In the left column, we illustrate two archetypical situations when performing single-molecule break junction experiments: Either no molecule incorporates into the junction and we only have Au−Au atomic junction where the conductance is $G \geq 1\ G_0$ (black box—third column) or a molecule will incorporate into the junction, and we will measure $G < 1\ G_0$ (red and blue boxes). For the situation with an incorporated molecule, two more qualitatively different situations exist: the molecule forms a strong chemical bond with Au, potentially pulling out the Au atoms of the Au tip during the evolution of the junction (red box). Or the molecule forms a weak dative bond that breaks at the Au−anchor interface during the evolution of the break junction (blue box). As the flicker noise differs between situations in which an Au−Au bond or a dative bond is broken (illustrated by the scatter plots in the final column), this method can be used to delineate between different binding situations.

spectroscopic properties of the Au−S interface.[7,28,29] A simple description of the Au−S bond as either covalent or ionic fails to explain its properties and oversimplifies the complex bonding scenario.[28,29] The best description of the Au−S bond can be thought of as a resonance hybrid with varying proportions of dispersive-force-dominating Au(0)-thiyl and covalent/ionic-force-dominating Au(I)-thiolate character.[7,28,29] The energies of these contributing resonance forms change with the environmental conditions, thus the ground state resultant hybrid can vary between these two extreme forms, often with one prevailing over the other.[7,28,29] Both of these chemically and physically driven contributing structures are themselves resonance hybrids of other canonical forms, often depending upon the hybridization of the Au atom.[29]

Experimental studies and electronic structural calculations have reported the signatures of the contributing canonical structures with their contributing proportions changing with environmental conditions.[19−22,28−30] In the case of Au compounds, the Au(I)-thiolate character dominates due to Au-s orbital binding to S, while for Au nanoparticles and Au surfaces, the bonding is closer to Au(0)-thiyl in character due to the preferential Au-d orbital binding to S. Nevertheless, due to these complexities, there are numerous discrepancies between the findings of various experimental and theoretical groups. However, it is widely accepted that the formation of Au−S bond with a deprotonated thiyl radical (RS) leads to a stronger chemisorption bond (hereafter referred to as an Au−SR bond) than that formed with a protonated RSH group, leading to a weaker coordinate (or dative) bond (hereafter referred to as Au−SRR′).[6,26,31] It has also been observed that the Au−S bond is stronger than that of the surface Au−Au bonds, and therefore the formation of Au−S affects the Au−Au bonding and geometry at the surface.[7,32−34] Numerous studies have investigated the rupture mechanism of the Au−S bond, for instance, by using atomic force microscopy (AFM)-based surface molecular force spectroscopy. Rupture force quantifies the strength of the bond and thus can differentiate between the Au−SR and Au−SRR′ bonding scenarios (Figure 1). A

https://doi.org/10.1021/jacs.3c14079
J. Am. Chem. Soc. XXXX, XXX, XXX−XXX

number of these studies,[35−37] performed on alkanethiols, demonstrated a rupture force of about 1.2 ± 0.3 nN. Molecular dynamic simulations[38] and break junction experiments[36,39] have demonstrated that, while pulling a thiol, an Au atom can get pulled from the surface, leading to Au−Au bond breakage with a rupture force of about 1.2−1.5 nN. Pulling an Au atom from the surface is plausible in light of previous reports that the strength of the Au−SR bond is stronger than that of an Au−Au bond at the surface, as the rupture force of an Au−Au bond is about 1.4 nN.[37,40] On the other hand, other AFM-based experiments[37,41] have reported a bond rupture force of less than 1.2 nN for similar experiments, leading to ambiguity.

One of the possible reasons for the substantial variation in experimental results could be the difference in environmental conditions under which the studies were performed, thus giving a range of rupture force values, as demonstrated by Xue et al.[31] Similarly, substantial variations have been found in single-molecule conductance values for thiol anchoring group-based molecular junctions.[6,42−44] This further strengthens the assertion that the nature of the Au−S and Au−Au bonds and the surface structure of Au are highly dynamic under different conditions, often leading to inconsistent experimental observations between different studies. To resolve this inconsistency in the experimental results, a new experimental approach is needed to probe these complicated Au−S interfaces and clarify our understanding. One such tool that takes advantage of correlating the electronic coupling and Au−Au/Au−anchor interface changes is the flicker noise analysis of single-molecule junctions. Figure 1 summarizes the events and the corresponding experimental observations upon junction evolution involving different types of interelectrode interactions during break junction experiments.

Introduced by Adak et al.,[45] flicker noise analysis in single-molecule junctions is primarily used to differentiate between through-bond and through-space tunneling. Flicker noise has served as a great tool to probe the electronic interactions in single-molecule junctions, including studies of quantum interference[46] and $\pi-\pi$ or $\sigma-\sigma$ stacking.[47,48] Flicker noise in break junctions builds upon the established toolbox employed in conventional electronics which study $1/f$ noise to model low-frequency fluctuations in the spectral density of a current signal.[49]

Using the mechanically controlled break junction (MCBJ) technique, herein, we probe the conductance and analyze the flicker noise for several aliphatic and aromatic thiols and thioethers. We demonstrate that flicker noise can be used to unambiguously differentiate between stronger chemisorption (Au−SR) and weaker coordinate (Au−SRR′) type interactions and also to probe the corresponding interfacial Au rearrangements in single-molecule break junction experiments. Furthermore, we show that thiols lose their H upon binding with Au to form the stronger Au−SR bond that leads to interfacial Au rearrangement, irrespective of the backbone of the molecule forming the junction, even though the molecular backbone can have a profound effect on the Au−S coupling strength in single-molecule junctions that in turn affects the strength of the Au−S bond.[50] The flicker noise measurements indicate that the Au rearrangement in Au−SR junctions resembles that of Au rearrangement in pure Au−Au metal contact breaking, irrespective of the molecular backbone. In contrast, thioethers show the formation of a weaker Au−SRR′ type bond, and the flicker noise measurements indicate changes in the Au/anchoring group interface, but not the Au−Au rearrangement like in the Au−SR case.

We also demonstrate that in the case of cyclic thioethers, the cyclic ring containing S can be opened under mild environmental conditions and is catalyzed by an interfacial electrical field. Under normal circumstances, cyclic thioethers are very stable and do not undergo hydrolysis. The cyclic thioether ring can only be opened under harsh chemical conditions.[51−53] By employing *in situ* conductance and flicker noise measurements, we monitored the ring-opening reaction of cyclic thioether under the influence of an interfacial electric field at the metal/molecule nano constriction and probed the corresponding interfacial changes during the evolution of the reaction. These observations open a chemical pathway to tune the electrode−molecule interactions (physisorption to chemisorption) at the interface and our results establish single-molecule break junction flicker noise as a reliable new method to probe interfacial reactions and interactions.

RESULTS AND DISCUSSION

The conductance of a molecule in a break junction is determined by the coupling strength and energy-level alignment of the frontier orbitals with the Fermi energy of the metal electrodes.[54,55] The coupling strength and the Fermi level alignment, in turn, are heavily influenced by the anchoring species.[8,56−59] Hence, to probe the Au−S interactions, we first performed single-molecule conductance measurements.

Conductance measurements were performed using our custom-developed mechanically controlled break junction setup (MCBJ, Figures 2A, S6, and S7).[60] More than 1500 conductance-displacement traces were recorded for each molecular system by repeated formation of molecular junctions using atomically sharp electrodes. The data was compiled without any data selection (see the Supporting Information for further details on the setup and measurement procedure). We used 4,4′-(ethene-1,2-diyl)dibenzenethiol (**A1**) and 1,2-bis(4-(methylthio)phenyl)ethene (**A2**) as initial model systems (Figure 2B). 1D conductance histograms of the two molecular systems are shown in Figure 2D. The data exhibit a sharp peak at 1 $G_0 \approx 77.5$ μS, which corresponds to the conductance of a single Au−Au atom point contact. After the Au atomic contact rupture, the Au atoms retract quickly, producing the Au snapback region, where the conductance decreases rapidly. In the case a molecular species incorporates into the junction, molecular conductance plateaus can be seen. Numerous traces with similar molecular plateaus yield a peak in the 1D conductance histogram, which can be fitted by a Gaussian distribution whose mean is the most probable single-molecule conductance.

Comparing the 1D histograms in Figure 2D, the conductance of **A1** ($10^{-1.95}$ G_0) is higher than that of **A2** ($10^{-2.7}$ G_0) by more than half an order of magnitude. As the molecular backbone (stilbene) is the same in both cases, the conductance change can be attributed to the difference in the coupling strength of the anchoring groups with the electrodes. The higher conductance of **A1** can be an indication that the S in **A1** binds stronger to Au via Au−SR type interactions after losing its H (forming **A0**, Figure 2C)[6] compared with that of **A2**, which binds via weaker Au−SRR′ type physisorption interactions.[6,61] The conductance value is consistent with the reported literature.[45,61]

Further, we measured the plateau length values (Δz) of the conductance plateaus of **A1** and **A2**, which gives an estimate of

https://doi.org/10.1021/jacs.3c14079
J. Am. Chem. Soc. XXXX, XXX, XXX−XXX

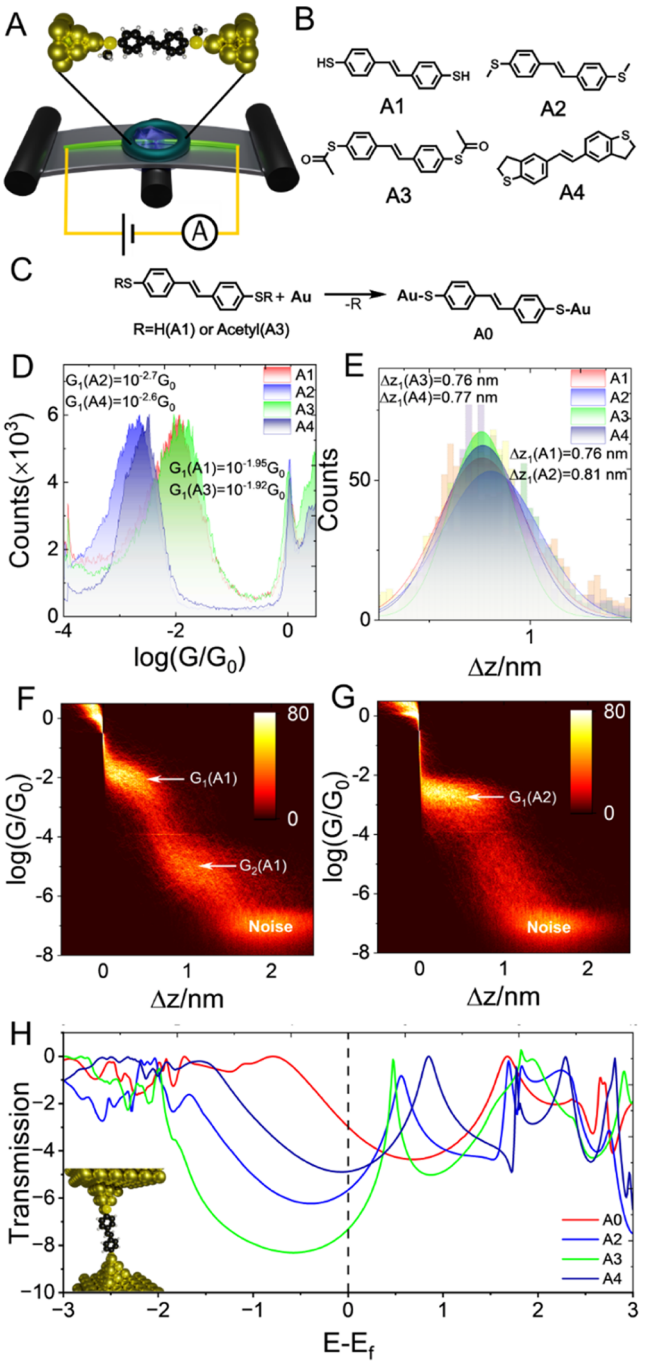

Figure 2. (A) Schematic representation of 3-point bending mechanism used in MCBJ setup. (B) Structure of A series molecules employed in this study. (C) Reaction illustrating the binding of S to Au by loss of its R-group (R = H or $-COCH_3$). (D) 1D conductance histograms, (E) Plateau length histograms of single-molecule junctions formed by A series molecules systems. 2D conductance histogram of (F) **A1** and (G) **A2**. Note the prominence of the G_2 (**A1**) plateau in (F). (H) Calculated electronic transmission of Au−molecule−Au junctions for **A0** (red), **A2** (blue), **A3** (green), and **A4** (royal blue). In the lower left corner is an illustration of the junction setup used for the transport calculations. The dashed black line is a guide to the eye for the Fermi level.

the maximum distance to which a molecular junction can be stretched before the Au−molecule−Au junction ruptures. This value correlates with the molecular length after adding the Au snapback distance (Δz_{corr}) of about 0.5 ± 0.1 nm.[62] As with molecular conductance, a 1D histogram of plateau lengths of numerous traces approximates a Gaussian distribution, whose mean correlates with the most probable molecular junction length (z). Since the molecular structures of **A1** and **A2** have the same backbone, and near similar anchor-to-anchor lengths, it is expected that both molecules yield similar mean plateau lengths (Δz). From Figure 2E, we see that the mean plateau lengths for **A1** and **A2** are 0.76 ± 0.2 and 0.81 ± 0.2 nm, respectively, matching our expectations. After correction for snapback ($z = \Delta z + \Delta z_{corr}$), these results match with the theoretically calculated molecular junction length of about 1.29 nm for both **A1** and **A2**.

To further demonstrate the loss of H in **A1** upon binding with Au electrodes (forming **A0**, see Figure 2C), we probed the conductance of two other stilbene derivatives where the fate of S is already fixed, namely, S,S′-(ethene-1,2-diylbis(4,1-phenylene))diethanethioate (**A3**) and (1,2-bis(2,3-dihydrobenzo[*b*]thiophen-5-yl)ethene) (**A4**). It was shown in the literature that the S atoms in **A3** get deprotected with the elimination of acetyl groups when in interaction with sharp Au electrodes in break junction techniques (also forming **A0**),[57,62,63] thus the Au−S interface should behave similarly to that of **A1** as both of these molecules form the same chemical species upon junction formation (**A0**) (Figure 2C). In contrast, **A4** has cyclic thioether anchoring groups, which cannot undergo elimination of the alkyl group under normal circumstances, meaning it is expected to bind similarly to **A2**.

It is evident from Figure 2D that the conductance of **A1** and **A2** matches **A3** and **A4**, respectively, which strongly suggests that the Au−S interface in **A1** and **A3** is similar. Likewise, the conductance measurements suggest that the Au−S interface of **A2** and **A4** is also similar. Furthermore, the plateau lengths (Figure 2E) of all of the A series molecules are the same within the measurement error of the break junction technique. Both pieces of evidence suggest a common stilbene backbone is trapped between the Au electrodes, yielding the same molecular length irrespective of the anchoring group.

Figure 2F,G shows the 2D conductance histograms of **A1** and **A2**. Two distinct conductance plateaus can be seen in Figure 2F, where the second plateau corresponds to the formation of $Au(SR)_2$.[64] The two plateaus in Figure 2F yield two peaks in the full-scale 1D conductance histogram of **A1** (Figure S11). All of the molecular systems employed in this study having Au−SR type electrode−molecule interactions show this behavior of having two distinct conductance plateaus with comparable probabilities, while aromatic systems with weaker Au−SRR′ bond with electrode only show a less prevalent second low conductance peak, which can be correlated to a dimer formation (stabilized via aromatic $\pi-\pi$ interactions).[47,65]

In Figure 2H, we plot the Landauer transmission of fully extended **A0**, **A2**, and **A4**. Note that we also calculated and plotted transmissions for **A3** in its hypothetically protected forms for comparison. The more realistic predictions for the conductance of **A3** is represented by the transmission of **A0**, when both **A1** and **A3** are in their deprotected forms (**A0**) where S binds covalently to Au. We see that the trend of the calculated transmissions at the Fermi level matches well with the experimental conductance values, i.e., the conductance trend is predicted to be **A0** > **A2** ≈ **A4** ≫ **A3**. We note that DFT calculations tend to overestimate actual conductance values.[66]

https://doi.org/10.1021/jacs.3c14079
J. Am. Chem. Soc. XXXX, XXX, XXX−XXX

As the thiolate anchor group of **A1** and **A3** (equivalent to **A0**, Figure 2C) binds more strongly to Au than the thiomethyl anchor groups of **A2** and **A4**, we see that the resonances are broader for **A0**. We also see that because the backbones of **A2** and **A4** are identical and their anchor groups are similar, their resonances lie close to each other. Finally, we calculated the transmission for **A3** where the acetate does not cleave off (Figure 2H). When the anchor remains a thioacetyl group, the transmission at the Fermi energy is the lowest relative to the rest of the molecules in the A series. This very low predicted transmission is further evidence that if the acetyl group had remained on **A3**, we would expect the measured conductance to lie lower than the conductance of **A1**. The electronic transmission calculations further corroborate the experimental measurements, suggesting that **A1** and **A3** bind similarly to Au with an Au−SR bond, and that **A2** and **A4** bind similarly with the weaker Au−SRR′ bond.

To get a better understanding of the nature of the Au−S interfacial chemistry, we performed the flicker noise analysis of the conductance signal of molecular junctions. Flicker noise analysis aims to quantify the $1/f$ noise in single-molecule junctions that originates from many two-level fluctuations in conductance when the molecular junctions are stretched. These fluctuations arise due to configurational changes in the electrodes which lead to variations in electrode−molecule coupling, and thus to fluctuations in the measured conductance (Figure 3A).[45]

The idea in single-molecule break junction flicker noise analysis is to calculate a flicker noise power scaling exponent value, n, that minimizes the correlation between normalized flicker noise ($N{\cdot}P/G^n$) and average conductance, G, for thousands of junctions. The value of the scaling exponent is indicative of the type of electronic coupling which in turn depends on the junction structure. Previous studies have shown that for a Au−Au contact (atomic contact) the scaling exponent is ∼0.5, for molecular junctions with through-bond coupling its value is around ∼1.0, and for tunnel junctions or through-space coupled junctions is ∼2.0.[45] Please refer to the Supporting Information for further details on our flicker noise measurements and analysis procedure.

Figure 3B shows the 2D histogram of flicker noise power plotted against average conductance for molecular junctions formed by **A1** and the red curve in Figure 3F shows the variation of Pearson's r value with scaling exponent (see the Supporting Information for further details on measurement and analysis procedure of flicker noise data). It is evident from the plot that the value for **A1** which minimizes the correlation between the flicker noise power and conductance is 0.53 (red curve in Figure 3F), which closely corresponds to that of metal−metal atomic contacts (∼0.51, black dotted line in Figure 3F,G).

As discussed above, the strength of Au−SR interactions is higher than that of Au−Au metal interactions; thus, we expect that the variation in conductance of these junctions is due to the Au rearrangement itself and not due to the variations in the Au−S coupling as those variations are being constrained due to strong Au−SR interactions. Thus, under these circumstances, the noise power factor of the Au−SR bonded junctions is comparable with that of Au−Au metal contacts (that is, n ∼0.5), where the source of the fluctuations is the Au atom rearrangements within the junction cross-section area (proportional to the square root of conductance).

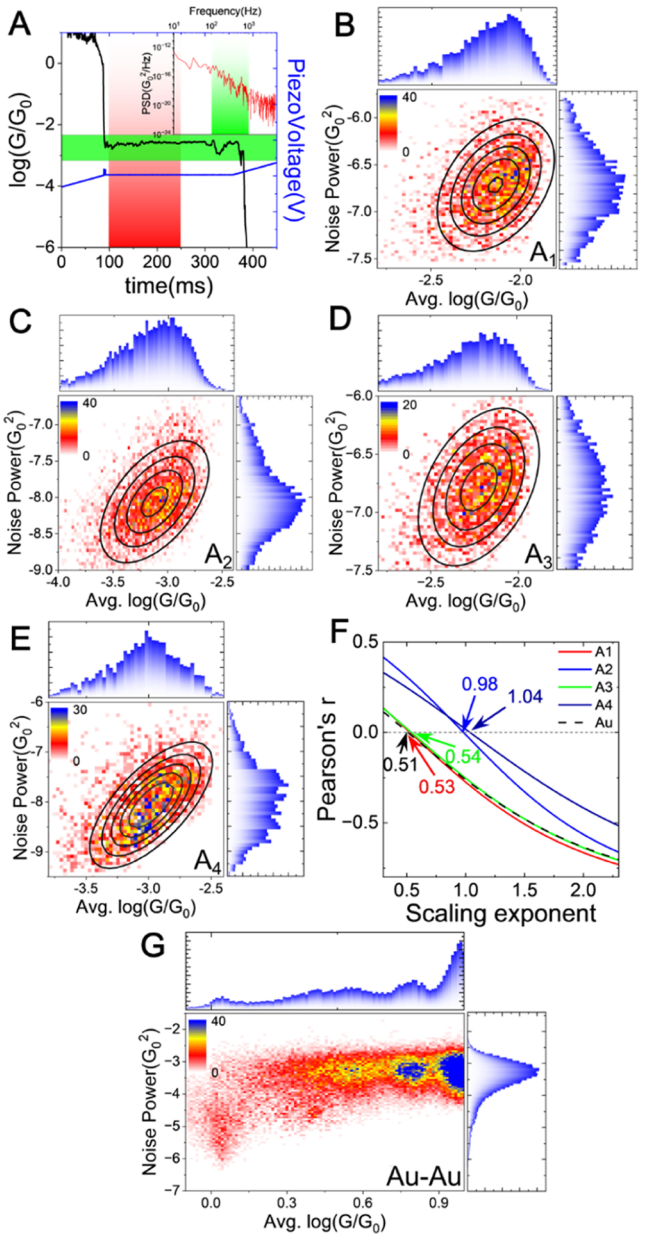

Figure 3. (A) Piezo ramp as a function of time (blue line) and the corresponding single-molecule conductance trace recorded for noise power analysis (black line). The red area shows the portion of conductance trace selected for further analysis, and the green area shows the conductance with standard deviation (for A2). Inset: power spectral density of the data portion selected, and the green area represents the 100−1000 Hz region between which the power spectral density is integrated to get flicker noise power value. 2D histogram of flicker noise (noise power (G_0^2)) against average conductance (avg. log(G/G_0)) of molecular junctions formed by (B) **A1**, (C) **A2**, (D) **A3**, and (E) **A4.** (F) Plot of linear (Pearson's) correlation coefficient against value of scaling exponent for various molecular junctions and Au metal atomic contacts and (G) 2D histogram of flicker noise (noise power (G_0^2)) against average conductance for Au atomic contacts with conductance from 10 G_0 to 1 G_0.

Next, we measured the flicker noise power of the **A2** molecule (Figure 3C) where the Au−S interactions are of the weak physisorption type (Au−SRR′). The blue curve in Figure

https://doi.org/10.1021/jacs.3c14079
J. Am. Chem. Soc. XXXX, XXX, XXX−XXX

3F shows the variation of Pearson's r with scaling exponent for **A2** and the value at near zero correlation is 0.98.

This value is in agreement with the values reported for molecular junctions with through-bond conductance with similar molecular structures, where the fluctuations in the conductance of these junctions are due to the variations in the Au−S coupling.[45] This change in the flicker noise scaling component of 0.53 to 0.98 from **A1** to **A2** further indicates the different nature of Au−S bonding in these two systems. As the conductance data (Figure 2C) suggested that **A1** and **A3** molecular junctions have a similar strong Au−SR interface (**A0**, Figure 2), while **A2** and **A4** molecular junctions show weak physisorption Au−SRR′ interface, the same is supported by their flicker noise analysis as well.

Figure 3D,E shows the 2D histogram of flicker noise plotted against average conductance for **A3** and **A4** molecular junctions, respectively (note that the flicker noise measurements for **A4** were performed in TCB solvent only, while for the other molecules, a 1:4 ratio of THF and TCB was used due to reasons mentioned later). Figure 3F shows the variations of correlation factor for all of these four stilbene derivatives, and it is evident that the scaling exponent value of **A3** (0.54, green curve) is close to that of **A1** (0.53, red curve) and the value of **A4** (1.04, royal blue curve) is close to that of **A2** (0.98, blue curve).

From these experimental observations, it is apparent that the noise power analysis can differentiate between different Au−S binding scenarios (Au−SR and Au−SRR′). It further confirms that Au−SR interactions are stronger than that of surface Au−Au interactions in single-molecule junctions and it is the Au−Au linkages that break and not the Au−S bonds in the case of **A0** (**A1** and **A3**) during the break junction experiments. In contrast, the Au−S bond breaks in the case of **A2** and **A4**, not the Au−Au bond.

Ring Opening of Cyclic Thioether. Cyclic thioether anchoring groups are commonly used in single-molecule conductance measurements due to their well-defined junction geometry leading to well-defined conductance histograms.[8,58,67] Surprisingly, when we probed the conductance of **A4** at 100 mV bias in THF/TCB (1:4, v/v) for a longer period of time (about 24 h), we observed a shift in the single-molecule conductance peak from $10^{-2.6}$ to $10^{-2.2}$ G_0 (Figure 4B). Interestingly, the conductance of **A4** after 24 h matches that of **A0** (deprotected form of **A1** and **A3**). Under the given experimental conditions, a small amount of H_2O present in the solvent might be sufficient to hydrolyze the thioether rings to a thiol derivative (**A4**-H) under the influence of an interfacial electrical field (100 mV to 10^8 V/m). These observations were further corroborated by NMR experiments where no evidence for cyclic thioether ring opening was found under similar environmental conditions but in the absence of bias voltage (Figure S18). The effect of the interfacial electric field on catalyzing the reaction has been shown to drive several reactions at such interfaces.[10,68,69]

To further prove our assumption of cyclic thioether ring opening, we performed a flicker noise analysis for **A4** using a freshly prepared solution of **A4** in THF/TCB (1:4, v/v) at 100 mV. Figure 4C shows the 2D histogram of flicker noise against the average conductance. As can be seen in the figure, two distinct regions of high counts are evident. These two regions correspond to two different chemical species probed during the course of measurement (24 h). We hypothesize that the initial molecular junctions were formed with cyclic thioether as the

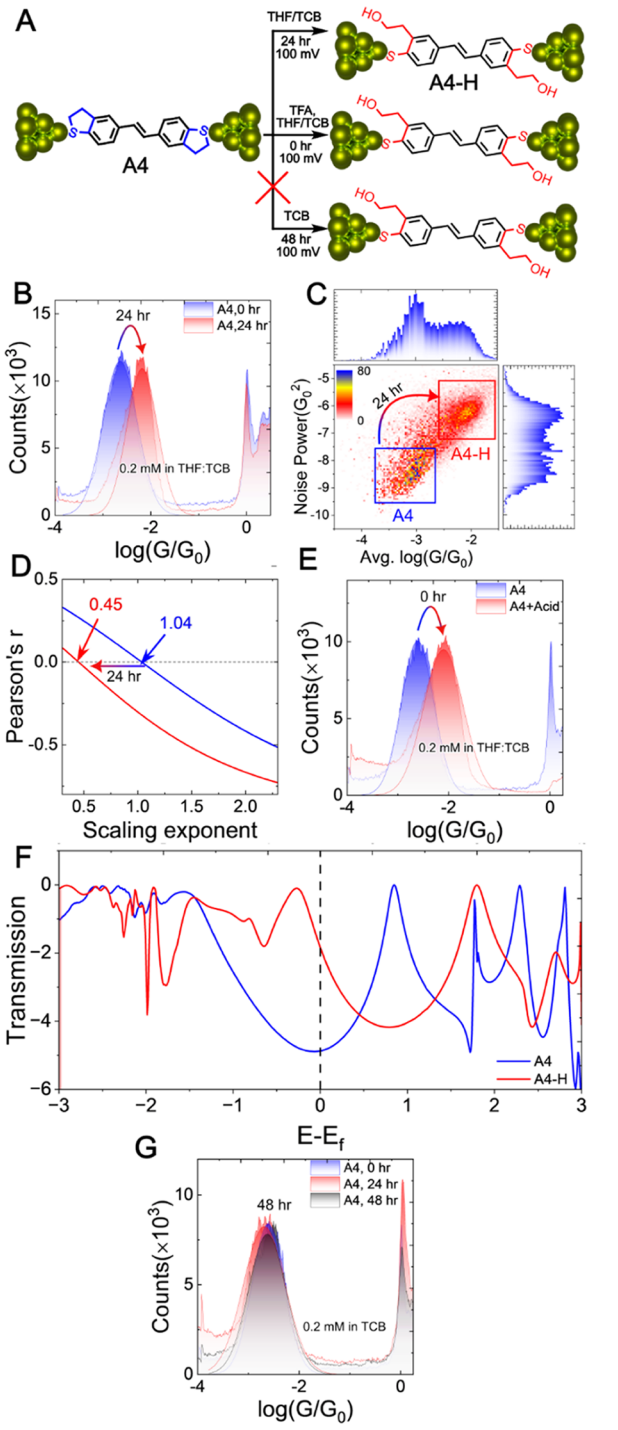

Figure 4. (A) Thioether ring opening of **A4** under different conditions. (B) 1D conductance histogram of **A4** measured immediately after solution preparation in THF/TCB (1:4, v/v) and after 24 h. (C) Flicker noise against average conductance for **A4** molecular junctions in THF/TCB (1:4, v/v). Note the two distinctive regions in the histogram. (D) The correlation coefficient plotted against the value of the scaling component for the two regions observed in (C). The color of the graphs corresponds to the color of the squares overlaid in (C). (E) 1D conductance histogram of **A4** before and after adding acid to the MCBJ cell. (F) Calculated electronic transmission of Au−molecule−Au junctions for **A4** (blue) and **A4**-H (red). The dashed black line is a guide to the eye for the Fermi level. (G) 1D conductance histogram of **A4** measured immediately after solution preparation in TCB only and after 48 h.

https://doi.org/10.1021/jacs.3c14079
J. Am. Chem. Soc. XXXX, XXX, XXX−XXX

anchoring group, and as time passed, the molecular junctions are formed with **A4**-H instead of **A4**. This hypothesis explains the two discrete regions in the noise power histogram and a corresponding shift in molecular conductance: a lower conductance region corresponding to **A4** (blue box in Figure 4C) and a higher conductance region corresponding to **A4**-H (red box in Figure 4C).

We then separated the two regions of the flicker noise plot and performed separate normalization to obtain the scaling exponent of the two regions separately. As seen from Figure 4D, the value of the scaling components of the two regions are 1.05 for **A4** (blue line in Figure 4D) and 0.45 for **A4**-H (red line in Figure 4D). These values of the scaling factor suggest the cyclic ring opened with time under the influence of an interfacial electric field and small amounts of H_2O present in the solvent which resulted in a change in the interfacial thiol binding from Au−SRR′ (weak physisorption of cyclic thioether, **A4**) to direct Au−SR (strong chemisorption with thiol, **A4**-H) like bond formation (Figure 4A). To further verify the thioether ring hydrolysis theory, we checked the influence of acid on the reaction catalyzed by an interfacial electric field. For this, we first measured the conductance of freshly prepared solution of **A4** in THF/TCB (1:4, v/v) and then 2 equiv of trifluoroacetic acid was added into the MCBJ cell and the conductance measurement was started again. Figure 4E shows the 1D conductance histogram of **A4** before (blue) and after (red) the acid was added. The resulting histograms closely resemble the measurement shown in Figure 4B. To benchmark the role of water, we performed conductance measurements in nonhygroscopic solvent (TCB) only and the resultant conductance data showed no change even after 48 h (Figure 4G). This experimental observation confirms the *in situ* cyclic thioether ring-opening reaction in the presence of water catalyzed by the electrical field. This case study demonstrates the unique capability of *in situ* single-molecule break junction experiments to catalyze and probe interfacial reactions at the nanoscale, when aided by flicker noise analysis.

In Figure 4F, we plot the Landauer transmission of fully extended **A4** and **A4**-H. The trend of the calculated transmissions matches well with the experimental conductance values. We note that despite **A4**-H having a resonance close to the Fermi energy, it is likely due to the inaccuracy of DFT to determine the exact energetic placement of the frontier molecular orbitals. This corroborates the evidence that the thioether ring opens to enable the formation of an Au−SR bond.

Effect of Nature, Length, Aromaticity, and Molecular Backbone on the Au−S Interfacial Chemistry. As the molecular backbone can have profound effects on molecule−metal coupling in single-molecule junctions,[50] we explored the effect of molecular backbone on Au−S bond strength in single-molecule junctions. Our goal was to see whether the strong Au−SR bonded interface is present in all thiols and weaker physisorption Au−SRR′ bonding in thioethers with different molecular backbones. For this, we probed the conductance and flicker noise of a range of thiol- and thioether-containing systems with a different backbone compared with the A series molecules. These systems include molecules with a short aromatic backbone (B series in Figure 5A), an aliphatic backbone (C series in Figure S29A), and a long aromatic backbone (D series in Figure S29A).

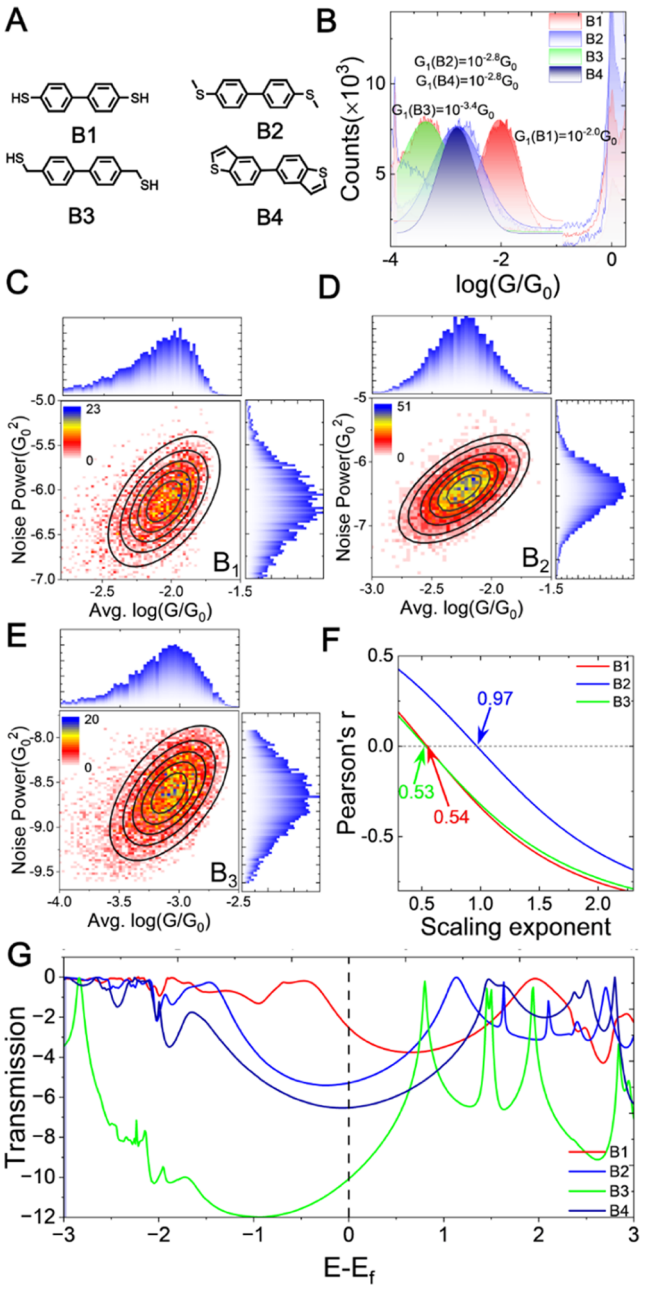

Figure 5. (A) Structures of the B series molecules. (B) 1D conductance histogram of B series biphenyl molecular variants. 2D histogram of noise power against the average conductance of (C) **B1**, (D) **B2**, and (E) **B3**. (F) The correlation coefficient plotted against the value of the scaling exponent for **B1**, **B2**, and **B3** molecular junctions. (G) Calculated electronic transmission of Au−molecule−Au junctions for **B1** (red), **B2** (blue), **B3** (green), and **B4** (royal blue). The dashed, black line is a guide to the eye for the Fermi level.

Among the molecules with a short aromatic backbone, we explored the following: [1,1′-biphenyl]-4,4′-dithiol (**B1**), 4,4′-bis(methylthio)-1,1′-biphenyl (**B2**), [1,1′-biphenyl]-4,4′-diyl-dimethanethiol (**B3**), and 5,5′-bibenzo[*b*]thiophene (**B4**). The chemical structures of these molecules are shown in Figure 5A. The conductance histograms of the molecular junctions formed by these compounds are shown in Figure 5B. It is apparent from Figures 5B and 2C that the conductance trend is similar to that of the A series molecules. The most probable conductance of **B1** is $10^{-2.7}$ G_0 due to the stronger Au−SR

https://doi.org/10.1021/jacs.3c14079
J. Am. Chem. Soc. XXXX, XXX, XXX−XXX

coupling compared with the rest of the molecules in the series. As expected, the conductances of **B2** and **B4** are close to equal due to their similar coupling strength and molecular backbone. However, the conductance of **B3** is the lowest, even though there are strong Au−S interactions. This happens due to the methylene groups between the thiol anchor and the benzene rings, which increases the tunneling gap leading to a substantial decrease in conductance. The same trend is reflected in the plateau length histograms of the corresponding molecular junctions (Figure S22B). Even though the conductance of **B2** and **B4** is the same, the junction formation probability for **B4** is smaller compared with **B2** as is apparent from the 2D conductance histograms of the corresponding molecular junctions (Figures S26−S28).

To further explore the Au−S bonding strength for these short aromatic systems, we analyzed the flicker noise power of their molecular junctions. Figure 5F shows the Pearson's r variation with scaling exponent. From this plot, we can see that the scaling exponent for **B1** and **B3** is similar and close to Au−Au atomic contacts as expected while that of **B2** is close to that of the molecular junctions with weak physisorbed Au−SRR′ interactions. Even though the conductance of **B1** and **B3** is more than an order of magnitude different, their similar scaling exponent highlights the ability of noise power analysis in identifying the similarities in the nature of binding (i.e., Au−SR). The same conclusions cannot be inferred from the conductance measurements alone. We could not evaluate the flicker noise power of **B4** due to the extremely low junction formation probability of the **B4** molecule. This made it impractical to obtain enough successful molecular junctions for noise power analysis.

In Figure 5G, we plot the Landauer transmission of fully extended **B1**, **B2**, **B3**, and **B4**. Although **B4** is predicted to have a slightly lower electronic transmission than **B2**, the overall trend matches the experimental trend. This discrepancy is likely due to the fact that transmission calculations are only of a single configuration, whereas the experiment samples a large variety of configurations. Choosing a fully extended, geometry-optimized junction structure generally matches the average conductance of experiments though slight variations will occur.

We also explored the aliphatic systems, namely, hexane-1,6-dithiol (**C1**) and 1,6-bis(methylthio)hexane (**C2**), and longer aromatic systems like [1,1′:4′,1″-terphenyl]-4,4′-dithiol (**D1**) and 4,4′-bis(methylthio)-1,1′:4′,1″-terphenyl (**D2**) (Figure S29A). The conductance and noise power analyses of these systems are summarized in Figure S29. It can be clearly interpreted from Figure S29B,C that irrespective of the molecular backbone aliphatic or aromatic, the conductance of thiol derivative is always higher than that of its thioether counterpart due to the stronger Au−SR interaction in thiol derivatives. The same is reflected in the flicker noise power analysis of their molecular conductance traces (Figure S29D). In Figure S29E, we plot the Landauer transmission of fully extended **C1**, **C2**, **D1**, and **D2**. Again, we see that the predicted trend for the electronic transmission matches well with the measured experimental conductance, i.e., the conductances of **C1** > **C2** and **D1** > **D2**.

All of the measurements described above demonstrated that it is the Au−Au bond that breaks when Au−SR interactions are involved (corresponding to the noise power value of ≈0.5), while few AFM-based studies have shown less rupture force for similar experiments than is required to break the Au−Au bond (1.4 nN). One of the many possible reasons for these discrepancies can be explained on the basis of the thermodynamic effect on measured rupture force among other environmental conditions. During AFM experiments, the rupture force depends on the force loading rate[70] ($r = dF/dt$) as well as on cantilever stiffness.[71] If the force is loaded slowly, the bond might break prematurely before maximally stretched due to thermal fluctuations resulting in less rupture force that is actually required to break the bond.[40] Thus, taking rupture force as a measure of bond strength might not be correct under these circumstances and will always show underestimated values. The rupture force is only a measure of the bond strength when the force loading rate is fast enough to ensure that thermal fluctuations play no role in the breaking process. Also, the rupture force is sensitive to the local temperature of the molecule−electrode interface which strongly depends on the applied bias.[70,72]

Further, in AFM studies, the rupture force is measured once a bond breaks; it is reasonable to argue that the rupture force depends on the initial, i.e., bonded and final broken states as well. Thus, its magnitude captures the signatures of both of these states. As a bond is being stretched, the resultant molecular states are stabilized by the surrounding environment, and these processes happen concurrently. Now depending on the environmental conditions, the product can be stabilized or destabilized upon breaking, which can lead to a change in rupture force. Instead, the flicker noise is measured while the bond is still intact experiencing some fluctuations due to the Au rearrangement in the electrode. As these measurements are from static junctions, the value of the noise is in fact a signature of the bonded state alone. Further, the events of any bond breakage due to thermal effects that would affect the flicker noise measurement are removed by ensuring that the conductance is still within the range of the molecular conductance. Hence, flicker noise can be a better tool in analyzing interfacial chemistry under these circumstances.

CONCLUSIONS

In this study, we have shown that flicker noise analysis can be a great tool in differentiating between strong chemisorbed Au−SR and weak physisorbed Au−SRR′ type of interfacial interactions irrespective of molecular backbone and the resulting conductance. Using a series of molecular systems, we have demonstrated that the strength of the Au−SR linkage is always higher than the Au−Au linkage irrespective of the nature of the molecular backbone (aromatic or aliphatic). As a result, flicker noise analysis has shown clear signatures for Au−Au bond breaking during the break junction experiments with thiol derivatives but not Au−S bond breaking. In contrast, thioethers displayed signatures for Au−S bond breaking during break junctions. We have demonstrated that it is not trivial to study the Au−S interfacial chemistry changes based on conductance measurements only. The measured noise scaling exponent of molecules with different conductance values but similar anchoring group chemistry highlights the ability of flicker noise power analysis in identifying the similarities in the nature of binding. The same conclusions cannot be inferred from the conductance measurements alone.

We further exploited the unique capabilities of single-molecule conductance and flicker noise measurements to probe interfacial chemical reactions at the single-molecule level. Typically, cyclic thioether anchoring groups are very stable under mild solvent conditions and have been widely

https://doi.org/10.1021/jacs.3c14079
J. Am. Chem. Soc. XXXX, XXX, XXX−XXX

used in several single-molecule conductance studies. Using *in situ* conductance and flicker noise measurements, we have observed the cyclic thioether ring opening. These results are complemented by the corresponding conductance measurements and theoretical calculations. This study illustrates that the single-molecule conductance, together with the flicker noise measurements, can be used to monitor and tune the chemical reactions at the single-molecule level.

■ ASSOCIATED CONTENT

Supporting Information

The Supporting Information is available free of charge at https://pubs.acs.org/doi/10.1021/jacs.3c14079.

Brief description of the synthesis and characterization of some compounds; Instrumental setup and measurement system; Complete conductance and flicker noise power data, measurement, and analysis procedure; and Computational methodology (PDF)

■ AUTHOR INFORMATION

Corresponding Authors

Keshaba N. Parida − *School of Chemistry, Indian Institute of Science Education and Research (IISER), Thiruvananthapuram 695551 Kerala, India;* orcid.org/0000-0003-3454-0868; Email: pkesh@iisertvm.ac.in

K. Geetharani − *Department of Inorganic and Physical Chemistry, Indian Institute of Science, Bangalore 560012, India;* orcid.org/0000-0003-2064-1297; Email: geetharani@iisc.ac.in

Joseph M. Hamill − *Department of Chemistry and Nano-Science Center, University of Copenhagen, DK-2100 Copenhagen Ø, Denmark*; Email: jmh@chem.ku.dk

Veerabhadrarao Kaliginedi − *Department of Inorganic and Physical Chemistry, Indian Institute of Science, Bangalore 560012, India;* orcid.org/0000-0002-4361-741X; Email: vkaliginedi@iisc.ac.in

Authors

Umar Rashid − *Department of Inorganic and Physical Chemistry, Indian Institute of Science, Bangalore 560012, India;* orcid.org/0000-0001-6583-061X

William Bro-Jørgensen − *Department of Chemistry and Nano-Science Center, University of Copenhagen, DK-2100 Copenhagen Ø, Denmark;* orcid.org/0000-0001-8171-6374

KB Harilal − *School of Chemistry, Indian Institute of Science Education and Research (IISER), Thiruvananthapuram 695551 Kerala, India;* orcid.org/0009-0004-2787-5357

PA Sreelakshmi − *Department of Inorganic and Physical Chemistry, Indian Institute of Science, Bangalore 560012, India;* orcid.org/0009-0001-8009-5825

Reetu Rani Mondal − *Department of Inorganic and Physical Chemistry, Indian Institute of Science, Bangalore 560012, India*

Varun Chittari Pisharam − *School of Chemistry, Indian Institute of Science Education and Research (IISER), Thiruvananthapuram 695551 Kerala, India*

Complete contact information is available at: https://pubs.acs.org/10.1021/jacs.3c14079

Notes

The authors declare no competing financial interest.

■ ACKNOWLEDGMENTS

V.K. and U.R. acknowledge the funding support from the Indian Institute of Science, DST-INSPIRE (DST/INSPIRE/04/2018/002983), SERB-Core research grant (CRG/2020/002302). U.R., PA.S., and R.R.M. acknowledge the financial support from the Prime Minister Research Fellowship (PMRF), Government of India. K.N.P. acknowledges CSIR for Pool Scientist [SRA, 13(9206-A)/2021-POOL]. This project has received funding from the European Research Council (ERC) under the European Union's Horizon 2020 Research and Innovation Programme (Grant Agreement No. 865870). The authors highly acknowledge Prof. Gemma C. Solomon, Dr. Gustav Wiberg, Dr. Garima Jindal, Dr. Vignesh Palani, and Prof. Latha Venkataraman for their useful comments and suggestions.

■ REFERENCES

(1) Saha, K.; Agasti, S. S.; Kim, C.; Li, X.; Rotello, V. M. Gold Nanoparticles in Chemical and Biological Sensing. *Chem. Rev.* **2012**, *112* (5), 2739−2779.

(2) Zhang, L.; Wang, E. Metal Nanoclusters: New Fluorescent Probes for Sensors and Bioimaging. *Nano Today* **2014**, *9* (1), 132−157.

(3) Cagno, V.; Andreozzi, P.; D'Alicarnasso, M.; Jacob Silva, P.; Mueller, M.; Galloux, M.; Le Goffic, R.; Jones, S. T.; Vallino, M.; Hodek, J.; Weber, J.; Sen, S.; Janeček, E.-R.; Bekdemir, A.; Sanavio, B.; Martinelli, C.; Donalisio, M.; Rameix Welti, M.-A.; Eleouet, J.-F.; Han, Y.; Kaiser, L.; Vukovic, L.; Tapparel, C.; Král, P.; Krol, S.; Lembo, D.; Stellacci, F. Broad-Spectrum Non-Toxic Antiviral Nanoparticles with a Virucidal Inhibition Mechanism. *Nat. Mater.* **2018**, *17* (2), 195−203.

(4) Kong, F.-Y.; Zhang, J.-W.; Li, R.-F.; Wang, Z.-X.; Wang, W.-J.; Wang, W. Unique Roles of Gold Nanoparticles in Drug Delivery, Targeting and Imaging Applications. *Molecules* **2017**, *22* (9), 1445.

(5) Love, J. C.; Estroff, L. A.; Kriebel, J. K.; Nuzzo, R. G.; Whitesides, G. M. Self-Assembled Monolayers of Thiolates on Metals as a Form of Nanotechnology. *Chem. Rev.* **2005**, *105* (4), 1103−1170.

(6) Inkpen, M. S.; Liu, Z.; Li, H.; Campos, L. M.; Neaton, J. B.; Venkataraman, L. Non-Chemisorbed Gold−Sulfur Binding Prevails in Self-Assembled Monolayers. *Nat. Chem.* **2019**, *11* (4), 351−358.

(7) Häkkinen, H. The Gold−Sulfur Interface at the Nanoscale. *Nat. Chem.* **2012**, *4* (6), 443−455.

(8) Kaliginedi, V.; Rudnev, A. V.; Moreno-García, P.; Baghernejad, M.; Huang, C.; Hong, W.; Wandlowski, T. Promising Anchoring Groups for Single-Molecule Conductance Measurements. *Phys. Chem. Chem. Phys.* **2014**, *16* (43), 23529−23539.

(9) Reed, M. A.; Zhou, C.; Muller, C. J.; Burgin, T. P.; Tour, J. M. Conductance of a Molecular Junction. *Science* **1997**, *278* (5336), 252−254.

(10) Aragonès, A. C.; Haworth, N. L.; Darwish, N.; Ciampi, S.; Bloomfield, N. J.; Wallace, G. G.; Diez-Perez, I.; Coote, M. L. Electrostatic Catalysis of a Diels−Alder Reaction. *Nature* **2016**, *531* (7592), 88−91.

(11) Jago, D.; Liu, C.; Daaoub, A. H. S.; Gaschk, E.; Walkey, M. C.; Pulbrook, T.; Qiao, X.; Sobolev, A. N.; Moggach, S. A.; Costa-Milan, D.; Higgins, S. J.; Piggott, M. J.; Sadeghi, H.; Nichols, R. J.; Sangtarash, S.; Vezzoli, A.; Koutsantonis, G. A. An Orthogonal Conductance Pathway in Spiropyrans for Well-Defined Electrosteric Switching Single-Molecule Junctions. *Small* **2023**, No. 2306334.

(12) Aragonès, A. C.; Medina, E.; Ferrer-Huerta, M.; Gimeno, N.; Teixidó, M.; Palma, J. L.; Tao, N.; Ugalde, J. M.; Giralt, E.; Díez-Pérez, I.; Mujica, V. Measuring the Spin-Polarization Power of a Single Chiral Molecule. *Small* **2017**, *13* (2), No. 1602519.

(13) Xie, Z.; Shi, S.; Liu, F.; Smith, D. L.; Ruden, P. P.; Frisbie, C. D. Large Magnetoresistance at Room Temperature in Organic Molecular Tunnel Junctions with Nonmagnetic Electrodes. *ACS Nano* **2016**, *10* (9), 8571−8577.

(14) Andika, R.; Yamada, R.; Tada, H. Magnetoresistance Originated from the Au/S Interface in Au/1,6-Hexanedithiol/Au Single-Molecule Junctions at Room Temperature. *Phys. Chem. Chem. Phys.* **2023**, *25* (28), 18642−18645.
(15) Kühnle, A.; Linderoth, T. R.; Hammer, B.; Besenbacher, F. Chiral Recognition in Dimerization of Adsorbed Cysteine Observed by Scanning Tunnelling Microscopy. *Nature* **2002**, *415* (6874), 891−893.
(16) Senapati, S.; Lindsay, S. Recent Progress in Molecular Recognition Imaging Using Atomic Force Microscopy. *Acc. Chem. Res.* **2016**, *49* (3), 503−510.
(17) Fang, J.; Zhang, B.; Yao, Q.; Yang, Y.; Xie, J.; Yan, N. Recent Advances in the Synthesis and Catalytic Applications of Ligand-Protected, Atomically Precise Metal Nanoclusters. *Coord. Chem. Rev.* **2016**, *322*, 1−29.
(18) Xin, N.; Guan, J.; Zhou, C.; Chen, X.; Gu, C.; Li, Y.; Ratner, M. A.; Nitzan, A.; Stoddart, J. F.; Guo, X. Concepts in the Design and Engineering of Single-Molecule Electronic Devices. *Nat. Rev. Phys.* **2019**, *1* (3), 211−230.
(19) Heister, K.; Zharnikov, M.; Grunze, M.; Johansson, L. S. O. Adsorption of Alkanethiols and Biphenylthiols on Au and Ag Substrates: A High-Resolution X-Ray Photoelectron Spectroscopy Study. *J. Phys. Chem. B* **2001**, *105* (19), 4058−4061.
(20) Heister, K.; Zharnikov, M.; Grunze, M.; Johansson, L. S. O.; Ulman, A. Characterization of X-Ray Induced Damage in Alkanethiolate Monolayers by High-Resolution Photoelectron Spectroscopy. *Langmuir* **2001**, *17* (1), 8−11.
(21) Corbierre, M. K.; Lennox, R. B. Preparation of Thiol-Capped Gold Nanoparticles by Chemical Reduction of Soluble Au(I)−Thiolates. *Chem. Mater.* **2005**, *17* (23), 5691−5696.
(22) Chaudhuri, A.; Odelius, M.; Jones, R. G.; Lee, T.-L.; Detlefs, B.; Woodruff, D. P. The Structure of the Au(111)/Methylthiolate Interface: New Insights from near-Edge x-Ray Absorption Spectroscopy and x-Ray Standing Waves. *J. Chem. Phys.* **2009**, *130* (12), No. 124708.
(23) Poirier, G. E.; Pylant, E. D. The Self-Assembly Mechanism of Alkanethiols on Au(111). *Science* **1996**, *272* (5265), 1145−1148.
(24) Voznyy, O.; Dubowski, J. J.; Yates, J. T.; Maksymovych, P. The Role of Gold Adatoms and Stereochemistry in Self-Assembly of Methylthiolate on Au(111). *J. Am. Chem. Soc.* **2009**, *131* (36), 12989−12993.
(25) Nuzzo, R. G.; Zegarski, B. R.; Dubois, L. H. Fundamental Studies of the Chemisorption of Organosulfur Compounds on Gold (111). Implications for Molecular Self-Assembly on Gold Surfaces. *J. Am. Chem. Soc.* **1987**, *109* (3), 733−740.
(26) Lavrich, D. J.; Wetterer, S. M.; Bernasek, S. L.; Scoles, G. Physisorption and Chemisorption of Alkanethiols and Alkyl Sulfides on Au(111). *J. Phys. Chem. B* **1998**, *102* (18), 3456−3465.
(27) Jadzinsky, P. D.; Calero, G.; Ackerson, C. J.; Bushnell, D. A.; Kornberg, R. D. Structure of a Thiol Monolayer-Protected Gold Nanoparticle at 1.1 Å Resolution. *Science* **2007**, *318* (5849), 430−433.
(28) Reimers, J. R.; Ford, M. J.; Marcuccio, S. M.; Ulstrup, J.; Hush, N. S. Competition of van Der Waals and Chemical Forces on Gold−Sulfur Surfaces and Nanoparticles. *Nat. Rev. Chem.* **2017**, *1* (2), 0017.
(29) Reimers, J. R.; Ford, M. J.; Halder, A.; Ulstrup, J.; Hush, N. S. Gold Surfaces and Nanoparticles Are Protected by Au(0)−Thiyl Species and Are Destroyed When Au(I)−Thiolates Form. *Proc. Natl. Acad. Sci. U.S.A.* **2016**, *113* (11), E1424−E1433, DOI: 10.1073/pnas.1600472113.
(30) Zhang, P.; Sham, T. K. X-Ray Studies of the Structure and Electronic Behavior of Alkanethiolate-Capped Gold Nanoparticles: The Interplay of Size and Surface Effects. *Phys. Rev. Lett.* **2003**, *90* (24), No. 245502.
(31) Xue, Y.; Li, X.; Li, H.; Zhang, W. Quantifying Thiol−Gold Interactions towards the Efficient Strength Control. *Nat. Commun.* **2014**, *5* (1), No. 4348.
(32) Grönbeck, H. Thiolate Induced Reconstruction of Au(111) and Cu(111) Investigated by Density Functional Theory Calculations. *J. Phys. Chem. C* **2010**, *114* (38), 15973−15978.
(33) Maksymovych, P.; Voznyy, O.; Dougherty, D. B.; Sorescu, D. C.; Yates, J. T. Gold Adatom as a Key Structural Component in Self-Assembled Monolayers of Organosulfur Molecules on Au(111). *Prog. Surf. Sci.* **2010**, *85* (5−8), 206−240.
(34) Pensa, E.; Cortés, E.; Corthey, G.; Carro, P.; Vericat, C.; Fonticelli, M. H.; Benítez, G.; Rubert, A. A.; Salvarezza, R. C. The Chemistry of the Sulfur−Gold Interface: In Search of a Unified Model. *Acc. Chem. Res.* **2012**, *45* (8), 1183−1192.
(35) Grandbois, M.; Beyer, M.; Rief, M.; Clausen-Schaumann, H.; Gaub, H. E. How Strong Is a Covalent Bond? *Science* **1999**, *283* (5408), 1727−1730.
(36) Xu, B.; Xiao, X.; Tao, N. J. Measurements of Single-Molecule Electromechanical Properties. *J. Am. Chem. Soc.* **2003**, *125* (52), 16164−16165.
(37) Frei, M.; Aradhya, S. V.; Hybertsen, M. S.; Venkataraman, L. Linker Dependent Bond Rupture Force Measurements in Single-Molecule Junctions. *J. Am. Chem. Soc.* **2012**, *134* (9), 4003−4006.
(38) Krüger, D.; Fuchs, H.; Rousseau, R.; Marx, D.; Parrinello, M. Pulling Monatomic Gold Wires with Single Molecules: An Ab Initio Simulation. *Phys. Rev. Lett.* **2002**, *89* (18), No. 186402.
(39) Huang, Z.; Chen, F.; Bennett, P. A.; Tao, N. Single Molecule Junctions Formed via Au−Thiol Contact: Stability and Breakdown Mechanism. *J. Am. Chem. Soc.* **2007**, *129* (43), 13225−13231, DOI: 10.1021/ja074456t.
(40) Pobelov, I. V.; Lauritzen, K. P.; Yoshida, K.; Jensen, A.; Mészáros, G.; Jacobsen, K. W.; Strange, M.; Wandlowski, T.; Solomon, G. C. Dynamic Breaking of a Single Gold Bond. *Nat. Commun.* **2017**, *8* (1), No. 15931.
(41) Skulason, H.; Frisbie, C. D. Detection of Discrete Interactions upon Rupture of Au Microcontacts to Self-Assembled Monolayers Terminated with − $S(CO)CH_3$ or − SH. *J. Am. Chem. Soc.* **2000**, *122* (40), 9750−9760.
(42) Strange, M.; Lopez-Acevedo, O.; Häkkinen, H. Oligomeric Gold−Thiolate Units Define the Properties of the Molecular Junction between Gold and Benzene Dithiols. *J. Phys. Chem. Lett.* **2010**, *1* (10), 1528−1532.
(43) Wang, H.; Leng, Y. Gold/Benzenedithiolate/Gold Molecular Junction: A Driven Dynamics Simulation on Structural Evolution and Breaking Force under Pulling. *J. Phys. Chem. C* **2015**, *119* (27), 15216−15223.
(44) Li, C.; Pobelov, I.; Wandlowski, T.; Bagrets, A.; Arnold, A.; Evers, F. Charge Transport in Single Au | Alkanedithiol | Au Junctions: Coordination Geometries and Conformational Degrees of Freedom. *J. Am. Chem. Soc.* **2008**, *130* (1), 318−326.
(45) Adak, O.; Rosenthal, E.; Meisner, J.; Andrade, E. F.; Pasupathy, A. N.; Nuckolls, C.; Hybertsen, M. S.; Venkataraman, L. Flicker Noise as a Probe of Electronic Interaction at Metal−Single Molecule Interfaces. *Nano Lett.* **2015**, *15* (6), 4143−4149.
(46) Garner, M. H.; Li, H.; Chen, Y.; Su, T. A.; Shangguan, Z.; Paley, D. W.; Liu, T.; Ng, F.; Li, H.; Xiao, S.; Nuckolls, C.; Venkataraman, L.; Solomon, G. C. Comprehensive Suppression of Single-Molecule Conductance Using Destructive σ-Interference. *Nature* **2018**, *558* (7710), 415−419.
(47) Magyarkuti, A.; Adak, O.; Halbritter, A.; Venkataraman, L. Electronic and Mechanical Characteristics of Stacked Dimer Molecular Junctions. *Nanoscale* **2018**, *10* (7), 3362−3368.
(48) Feng, A.; Zhou, Y.; Al-Shebami, M. A. Y.; Chen, L.; Pan, Z.; Xu, W.; Zhao, S.; Zeng, B.; Xiao, Z.; Yang, Y.; Hong, W. σ−σ Stacked Supramolecular Junctions. *Nat. Chem.* **2022**, *14* (10), 1158−1164.
(49) Dutta, P.; Horn, P. M. Low-Frequency Fluctuations in Solids: 1 f Noise. *Rev. Mod. Phys.* **1981**, *53* (3), 497−516.
(50) Komoto, Y.; Fujii, S.; Nakamura, H.; Tada, T.; Nishino, T.; Kiguchi, M. Resolving Metal-Molecule Interfaces at Single-Molecule Junctions. *Sci. Rep.* **2016**, *6* (1), No. 26606.
(51) Zhang, R.; Li, Q.; Xie, Q.; Ni, C.; Hu, J. Difluorocarbene-Induced Ring-Opening Difluoromethylation-Halogenation of Cyclic (Thio)Ethers with $TMSCF_2X$ (X = Br, Cl)**. *Chem. − Eur. J.* **2021**, *27* (71), 17773−17779.

https://doi.org/10.1021/jacs.3c14079
J. Am. Chem. Soc. XXXX, XXX, XXX−XXX

(52) Zheng, T.; Tan, J.; Fan, R.; Su, S.; Liu, B.; Tan, C.; Xu, K. Diverse Ring Opening of Thietanes and Other Cyclic Sulfides: An Electrophilic Aryne Activation Approach. *Chem. Commun.* **2018**, *54* (11), 1303−1306.
(53) Fan, R.; Liu, B.; Zheng, T.; Xu, K.; Tan, C.; Zeng, T.; Su, S.; Tan, J. An Aryne Triggered Ring-Opening Fluorination of Cyclic Thioethers with Potassium Fluoride. *Chem. Commun.* **2018**, *54* (51), 7081−7084.
(54) Metzger, R. M. Unimolecular Electronics. *Chem. Rev.* **2015**, *115* (11), 5056−5115.
(55) Cuevas, J. C.; Scheer, E. *Molecular Electronics: An Introduction to Theory and Experiment*, 2nd ed.; World Scientific Series in Nanoscience and Nanotechnology; World Scientific, 2017; Vol. *15*.
(56) Chen, F.; Li, X.; Hihath, J.; Huang, Z.; Tao, N. Effect of Anchoring Groups on Single-Molecule Conductance: Comparative Study of Thiol-, Amine-, and Carboxylic-Acid-Terminated Molecules. *J. Am. Chem. Soc.* **2006**, *128* (49), 15874−15881.
(57) Frisenda, R.; Tarkuç, S.; Galán, E.; Perrin, M. L.; Eelkema, R.; Grozema, F. C.; Van Der Zant, H. S. J. Electrical Properties and Mechanical Stability of Anchoring Groups for Single-Molecule Electronics. *Beilstein J. Nanotechnol.* **2015**, *6*, 1558−1567.
(58) Moreno-García, P.; Gulcur, M.; Manrique, D. Z.; Pope, T.; Hong, W.; Kaliginedi, V.; Huang, C.; Batsanov, A. S.; Bryce, M. R.; Lambert, C.; Wandlowski, T. Single-Molecule Conductance of Functionalized Oligoynes: Length Dependence and Junction Evolution. *J. Am. Chem. Soc.* **2013**, *135* (33), 12228−12240.
(59) Daaoub, A.; Morris, J. M. F.; Béland, V. A.; Demay-Drouhard, P.; Hussein, A.; Higgins, S. J.; Sadeghi, H.; Nichols, R. J.; Vezzoli, A.; Baumgartner, T.; Sangtarash, S. Not So Innocent After All: Interfacial Chemistry Determines Charge-Transport Efficiency in Single-Molecule Junctions. *Angew. Chem., Int. Ed.* **2023**, *62* (24), No. e202302150.
(60) Rashid, U.; Chatir, E.; Medrano Sandonas, L.; Sreelakshmi, P.; Dianat, A.; Gutierrez, R.; Cuniberti, G.; Cobo, S.; Kaliginedi, V. Dithienylethene-Based Single Molecular Photothermal Linear Actuator. *Angew. Chem., Int. Ed.* **2023**, *62* (16), No. e202218767.
(61) Meisner, J. S.; Ahn, S.; Aradhya, S. V.; Krikorian, M.; Parameswaran, R.; Steigerwald, M.; Venkataraman, L.; Nuckolls, C. Importance of Direct Metal−π Coupling in Electronic Transport Through Conjugated Single-Molecule Junctions. *J. Am. Chem. Soc.* **2012**, *134* (50), 20440−20445.
(62) Kaliginedi, V.; Moreno-García, P.; Valkenier, H.; Hong, W.; García-Suárez, V. M.; Buiter, P.; Otten, J. L. H.; Hummelen, J. C.; Lambert, C. J.; Wandlowski, T. Correlations between Molecular Structure and Single-Junction Conductance: A Case Study with Oligo(Phenylene-Ethynylene)-Type Wires. *J. Am. Chem. Soc.* **2012**, *134* (11), 5262−5275.
(63) Hong, W.; Valkenier, H.; Mészáros, G.; Manrique, D. Z.; Mishchenko, A.; Putz, A.; García, P. M.; Lambert, C. J.; Hummelen, J. C.; Wandlowski, T. An MCBJ Case Study: The Influence of π-Conjugation on the Single-Molecule Conductance at a Solid/Liquid Interface. *Beilstein J. Nanotechnol.* **2011**, *2*, 699−713.
(64) Leary, E.; Zotti, L. A.; Miguel, D.; Márquez, I. R.; Palomino-Ruiz, L.; Cuerva, J. M.; Rubio-Bollinger, G.; González, M. T.; Agrait, N. The Role of Oligomeric Gold−Thiolate Units in Single-Molecule Junctions of Thiol-Anchored Molecules. *J. Phys. Chem. C* **2018**, *122* (6), 3211−3218.
(65) Frisenda, R.; Janssen, V. A. E. C.; Grozema, F. C.; van der Zant, H. S. J.; Renaud, N. Mechanically Controlled Quantum Interference in Individual π-Stacked Dimers. *Nat. Chem.* **2016**, *8* (12), 1099−1104.
(66) Evers, F.; Weigend, F.; Koentopp, M. Conductance of Molecular Wires and Transport Calculations Based on Density-Functional Theory. *Phys. Rev. B* **2004**, *69* (23), No. 235411.
(67) Park, Y. S.; Widawsky, J. R.; Kamenetska, M.; Steigerwald, M. L.; Hybertsen, M. S.; Nuckolls, C.; Venkataraman, L. Frustrated Rotations in Single-Molecule Junctions. *J. Am. Chem. Soc.* **2009**, *131* (31), 10820−10821.
(68) Zhang, B.; Schaack, C.; Prindle, C. R.; Vo, E. A.; Aziz, M.; Steigerwald, M. L.; Berkelbach, T. C.; Nuckolls, C.; Venkataraman, L. Electric Fields Drive Bond Homolysis. *Chem. Sci.* **2023**, *14* (7), 1769−1774.
(69) Wang, X.; Zhang, B.; Fowler, B.; Venkataraman, L.; Rovis, T. Alkane Solvent-Derived Acylation Reaction Driven by Electric Fields. *J. Am. Chem. Soc.* **2023**, *145* (22), 11903−11906.
(70) Huang, Z.; Xu, B.; Chen, Y.; Di Ventra, M.; Tao, N. Measurement of Current-Induced Local Heating in a Single Molecule Junction. *Nano Lett.* **2006**, *6* (6), 1240−1244, DOI: 10.1021/nl0608285.
(71) Hybertsen, M. S. Modeling Single Molecule Junction Mechanics as a Probe of Interface Bonding. *J. Chem. Phys.* **2017**, *146* (9), No. 092323.
(72) Huang, Z.; Chen, F.; D'agosta, R.; Bennett, P. A.; Di Ventra, M.; Tao, N. Local Ionic and Electron Heating in Single-Molecule Junctions. *Nat. Nanotechnol.* **2007**, *2* (11), 698−703.

https://doi.org/10.1021/jacs.3c14079
J. Am. Chem. Soc. XXXX, XXX, XXX−XXX